RESEARCH ARTICLE | MAY 11 2010

Transition paths in molecules at finite temperature

F. J. Pinski; A. M. Stuart

J. Chem. Phys. 132, 184104 (2010)
https://doi.org/10.1063/1.3391160

Transition paths in molecules at finite temperature

F. J. Pinski[1,a] and A. M. Stuart[2,b]
[1]*Department of Physics, University of Cincinnati, P.O. Box 210011, Cincinnati, Ohio 45221, USA*
[2]*Mathematics Institute, University of Warwick, Coventry CV4 7AL, United Kingdom*

(Received 21 May 2009; accepted 24 March 2010; published online 11 May 2010)

In the zero temperature limit, it is well known that in systems evolving via Brownian dynamics, the most likely transition path between reactant and product may be found as a minimizer of the Freidlin–Wentzell action functional. An analog for finite temperature transitions is given by the Onsager–Machlup functional. The purpose of this work is to investigate properties of Onsager–Machlup minimizers. We study transition paths for thermally activated molecules governed by the Langevin equation in the overdamped limit of Brownian dynamics. Using gradient descent in pathspace, we minimize the Onsager–Machlup functional for a range of model problems in one and two dimensions and then for some simple atomic models including Lennard-Jones seven-atom and 38-atom clusters, as well as for a model of vacancy diffusion in a planar crystal. Our results demonstrate interesting effects, which can occur at nonzero temperature, showing transition paths that could not be predicted on the basis of the zero temperature limit. However the results also demonstrate unphysical features associated with such Onsager–Machlup minimizers. As there is a growing literature that addresses transition path sampling by related techniques, these insights add a potentially useful perspective into the interpretation of this body of work. © *2010 American Institute of Physics*. [doi:10.1063/1.3391160]

I. INTRODUCTION

Many systems are observed to undergo phase transitions, or conformation changes, as some external field is altered. Very often such a transition is inhibited by the presence of an energy barrier. If the barrier is large compared to the temperature, the transition takes place on very long time-scales; it is these rare events that are of interest here. They are characterized by paths: sequences of configurations which are constrained to start in one state, or conformation, and end in another. We are then interested in sampling from the distribution of paths, that are so constrained, at small but nonzero temperatures. This problem has been widely studied, using a range of different dynamical models, and a range of different computational techniques. A recent overview of the subject may be found in Ref. 1. Models and algorithms based on classical Hamiltonian models of the dynamics are described in Refs. 2–4. Models and algorithms based on the Langevin equation, particularly in the overdamped limit of Brownian dynamics, may be found in Refs. 5–9. For more detailed literature review, the reader is pointed to these references.

Here we explore transitions paths for systems that evolve via the overdamped Langevin equation: the Brownian dynamics model. In the zero temperature limit it is well known that with overwhelming probability, transitions will be described by minimizers of the Freidlin–Wentzell action functional.[10] These transitions occur on infinitely long time intervals and are best computed by techniques that parametrize the paths intrinsically (using arc-length, say, Ref. 5) rather than using time. The transition paths thus calculated are smooth functions, unlike typical paths of Brownian dynamics, which are not differentiable, and the precise characterization of Freidlin–Wentzell minimizers is that they determine the centers of small tubes in pathspace, which account for the bulk of the probability, via the theory of large deviations. An analog for finite temperature transitions, over finite time intervals, is given by the Onsager–Machlup functional.[11] The purpose of this work is to investigate properties of Onsager–Machlup minimizers. We refer to the paths found this way as most probable paths, MPPs for short.

We study a range of simple examples, investigating the behavior of this approach to determining transitions at finite temperature and on finite time intervals, and exposing some of the pitfalls that arise from studying paths that identify the centers of small tubes which maximize probability. As many algorithms based on the Onsager–Machlup approach either specify the duration of transitions or leave it to be determined as part of the algorithm (see, e.g., Refs. 9 and 3), the studies in this paper may shed light on issues arising from the use of such algorithms. Recently Faccioli and co-workers[9,12–14] championed such dominant paths as a route to explore protein folding. The pitfalls shown in this work show how such investigations may be misleading and some indications of why. These pitfalls stem from the fact that MPPs cannot, in general, be considered physical, as we will demonstrate below with specific examples.

Our point of departure is *Brownian dynamics*,

[a]Electronic mail: frank.pinski@uc.edu.
[b]Electronic mail: a.m.stuart@warwick.ac.uk.

$$\frac{dx}{dt} = -\nabla V(x) + \sqrt{\frac{2}{\beta}}\frac{dW}{dt}. \tag{1}$$

Here $x \in \mathbb{R}^{nd}$ denotes the configuration of n atoms in $\mathbb{R}^d$, $V:\mathbb{R}^{nd} \to \mathbb{R}$ is the potential, and β is the (nondimensional) inverse temperature. The function W is a standard Brownian motion in $\mathbb{R}^{nd}$. We are interested in paths of this stochastic differential equation (SDE) conditioned to make a transition from configuration x^- to x^+ in a specified time U so that we have the boundary conditions

$$x(0) = x^- \quad \text{and} \quad x(U) = x^+. \tag{2}$$

Typically $x^{\pm}$ are local minima of V. Of particular interest to us will be the regime where the length of the path, U, is long.

In Sec. II we introduce the problem formulation, showing how the MPPs can be found from study of a simple problem in the calculus of variations. In Sec. III we describe the results of numerical experiments, which illustrate the analysis of the previous section, on test problems in one and two dimensions, a planar model of vacancy diffusion, and on various Lennard-Jones clusters in the plane and in three-dimensional Euclidean space.

The main points of the paper can be summarized as follows.

(i) The path length U is a parameter in this approach. For infinite or large inverse temperature β and as $U \to \infty$, the Onsager–Machlup approach recovers equilibrium statistical mechanics and the Fredilin–Wentzell minimizers. For small values of U, the constraint implied by the boundary conditions dominates the paths, and simple geometric connections between x^- and x^+ are found, with little physical effects from the potential. At intermediate values of U, a range of complex effects can occur, depending on the relationship between U and β; some are physical and some quite unphysical.

(ii) For long enough paths, the MPPs are segmented; they exhibit rapid transitions between extremal values of a function G (defined below), which we term the *path potential*. At large inverse temperature these extremals are critical points of V, i.e., minima, saddles, or maxima. At zero temperature the standard picture of an instanton connecting two minima does not hold; the instanton is broken into two, each connecting a minima to the saddle through which a transition is made. The length of time spent in any of the segments is somewhat arbitrary; the minimization differs only by exponentially small amounts as these times are varied. This picture is consistent with the zero temperature limit and Freidlin–Wentzell minimizers.

(iii) At temperatures above zero, the trace of the Hessian of the potential V (the sum of the eigenvalues of the linearized dynamics) comes into play. The effect of this term has myriad effects. In particular it can cause MPPs to spend the majority of their time at saddles, and it can shift the MPPs away from the extrema of V. We show that the latter shift can be large even at low temperatures. Furthermore, where two transition paths exist, the MPP is not necessarily the physically relevant one: The MPP may choose the path with lower entropic contributions to the probability flux. In the one-dimensional (1D) double well, a small asymmetry in the potential produces MPPs that exponentially overestimate the time spent in the deeper well.

As a consequence of our calculations reported in this paper, we conclude that numerical approaches that attempt to maximize probability on pathspace via the Onsager–Machlup functional should be treated cautiously.

II. PROBLEM FORMULATION

We start by asking the following question: How should we choose a smooth function x so that the probability of paths satisfying Eqs. (1) and (2) and lying in a small tube about x is maximized, asymptotically as the radius of the tube shrinks to zero? The answer is given as follows. Define the path potential, G, by

$$G(x;\beta) = \frac{1}{2}|\nabla V(x)|^2 - \frac{1}{\beta}\Delta V(x). \tag{3}$$

The Onsager–Machlup functional is then

$$I(x;\beta) = \frac{1}{2}\int_0^U \left|\frac{dx}{dt}\right|^2 dt + \int_0^U G(x;\beta)dt. \tag{4}$$

(Strictly speaking the Onsager–Machlup functional is $(\beta/2)I(x;\beta)$, but the constant of proportionality is not relevant in what follows.) Minimizers of this functional, subject to the boundary conditions (2), are termed MPPs, and they solve the desired probability maximization problem.[11] Studying the properties of these minimizers, for large inverse temperature β and for various choices of the transition time U, is the subject of this paper. For large U it is intuitive that minimization will tend to occur via solutions, which are approximately constant on minimizers of G and exhibiting rapid transitions (relative to time-scale U) between different such minimizers; we refer to this phenomena as *segmenting*. It is tempting to simply drop the term proportional to β^{-1} appearing in the path potential G when working at low temperatures. However, notice that in equilibrium,

$$\langle|\nabla V(x)|^2\rangle = \frac{1}{\beta}\langle\Delta V(x)\rangle = -\frac{1}{2}\langle G\rangle. \tag{5}$$

(Here angular brackets denote thermal equilibrium averages.) One can easily show the above by integrating by parts. Thus the two terms in G are typically the same order of magnitude.

It is instructive to see how the zero temperature limit is contained within this picture of probability maximizers at finite temperature. Note first that

$$I_0(x) = \lim_{\beta\to\infty} I(x;\beta)$$

may be written as

$$I_0(x) = I_a(x) + (V(x^+) - V(x^-)),$$

$$I_a(x) = \frac{1}{2}\int_0^U \left| \frac{dx}{dt} - \nabla V(x) \right|^2 dt.$$

Here $I_a(x)$ is simply the Freidlin–Wentzell action potential.[10] Using this fact it follows that if $U \to \infty$, then the minimizer of I_0 is given by a sum rule,

$$\sum_i |V(x_{i+1}) - V(x_i)|, \tag{6}$$

where the $\{x_i\}$ denote the extremal configurations of V visited by the MPP in the order visited. Thus, for $\beta \to \infty$ and then $U \to \infty$, the classical zero temperature limit is recovered. However, as is well known, such double limiting procedures can be very sensitive to the manner in which both parameters approach infinity. If we simply choose large β and U, different effects may occur, depending on the relative size of U and β. As we will see, some of these effects may be nonphysical.

III. NUMERICAL EXPERIMENTS

We illustrate the physical characteristics of the MPPs described in the previous section through the calculation of MPPs for a variety of test problems listed below. The first three are simple low-dimensional problems, which have the virtue of being easy to visualize. The remaining test problems are more realistic physical problems, which manifest similar behavior to that exemplified by the simple problems. We do not impose a specific relationship between temperature and path length in our study of MPPs; rather we vary β and U independently. However interesting mathematical insight into the problem can be obtained by letting U vary with β, and this analysis may be found in Ref. 15.

Critical points of I may be found via the partial differential equation (PDE)

$$\frac{\partial x}{\partial \tau} = \frac{\partial^2 x}{\partial t^2} - \nabla G(x;\beta), \tag{7a}$$

$$x(0,\tau) = x^- \quad \text{and} \quad x(U,\tau) = x^+, \tag{7b}$$

$$x(t,0) = x_0(t). \tag{7c}$$

This PDE performs a gradient descent for $I(x)$, and thus we may use discretizations of the PDE to find MPPs.

Simple finite difference expressions are used for both the first derivative (in τ) and the second derivative (in t). We use the Crank–Nicolson discretization to treat the linear part of the problem, which combines the space and time derivatives; the path potential contribution ∇G is treated explicitly. We use a grid in $t \in [0, U]$ with the order of 10^2–10^4 points; the exact number chosen is guided by the complexity of the solution. In the coordinate τ we used four modifications of the basic ensuing iterative method. The simplest method used was a relaxation procedure, where the step size was kept fixed. The second method was similar, except that the step size ($\Delta\tau$) is slowly adjusted upward whenever the result for I decreased; and when I increased, the iteration was rejected, and $\Delta\tau$ would be substantially decreased typically by a factor between 4 and 10. The third method employed was similar to that in Ref. 16 using five iterates to extract the next one. Finally, due to the slow movement of the interfaces between states, we sometimes adjusted the path by hand to advance these interfaces more quickly. In this paper, we are not trying to explore how efficiently such a numerical method finds the optimal pathway but rather to understand the behavior of the MPP itself. We used the zero temperature sum rule (6) as a numerical check when β and U are large; see Refs. 17 and 15. Whenever we refer to computations in the zero temperature limit, $\beta = \infty$, we refer to employment of the same iterative method based on discretization of a PDE, to minimize $I_0(x)$ directly.

A. Example 3.1: Double-well potential

We consider the 1D problem for a single particle x in one dimension and moving in a potential V,

$$V(x) = ax^4 + bx^3 - 2cx^2.$$

For this example, $n=d=1$. The choice $a=c=1$ and $b=0$ renders the problem symmetric. Small deviations from these values introduce slight asymmetry. This potential has, for $a > 0$ and $c > 0$, two minima and one maximum. For the asymmetric case, we use parameter values of $a=0.999\,993$, $b=-0.005$, and $c=0.999\,989$. These constants are chosen so that the barrier remains at $x=0$, the mean barrier is unity, the separation δx between the minima is 2, and the difference of the depths of the wells, δV, is 0.02.

First consider the symmetric double well. The zero temperature MPP on an infinitely long time interval is found as the minimizer of $I_0(x)$ in the limit as $\beta \to \infty$; see Ref. 10 for theoretical developments and Ref. 17 for applications. First we study the effect of finite time-interval effects on this MPP by minimizing I_0 on paths of length $U=1$, 2,5, 10, and 20. The results are summarized in Fig. 1(a). This illustrates the segmenting of the MPPs. At zero temperature ($\beta=\infty$) sufficiently long paths (the black curve in the figure) are segmented into approximately constant values given by critical points of $V(x)$. In this case two minima exist at $x=\pm 1$, and a maximum at $x=0$. In Fig. 1(b) we carry out similar calculations but now at finite temperature ($\beta<\infty$), minimizing $I(x)$. We again see the segmenting effect for long paths, but notice that now these paths spend very little time at the maximum $x=0$ and spend the most time at the two minima $x=\pm 1$. This is the traditional instanton picture. This effect demonstrates the importance of the trace of the Hessian of V, ΔV, in the path potential G since in this case, $\Delta V(x)$ is negative at $x^0=0$ and positive at $x^\pm = \pm 1$. Thus segmented minimizers, which concentrate at critical points of V, will prefer the minima over the maxima of V. It is also noteworthy that for sufficiently long paths, the difference between zero temperature and finite, but small, temperature is dramatic (black curves), while for short paths it is negligible (red curves).

We now add a small asymmetry using the parameters stated above. At zero temperature (minimizing I_0) the MPP is little changed by the asymmetry and almost indistinguishable from that found in the symmetric case—compare Fig. 1(c)

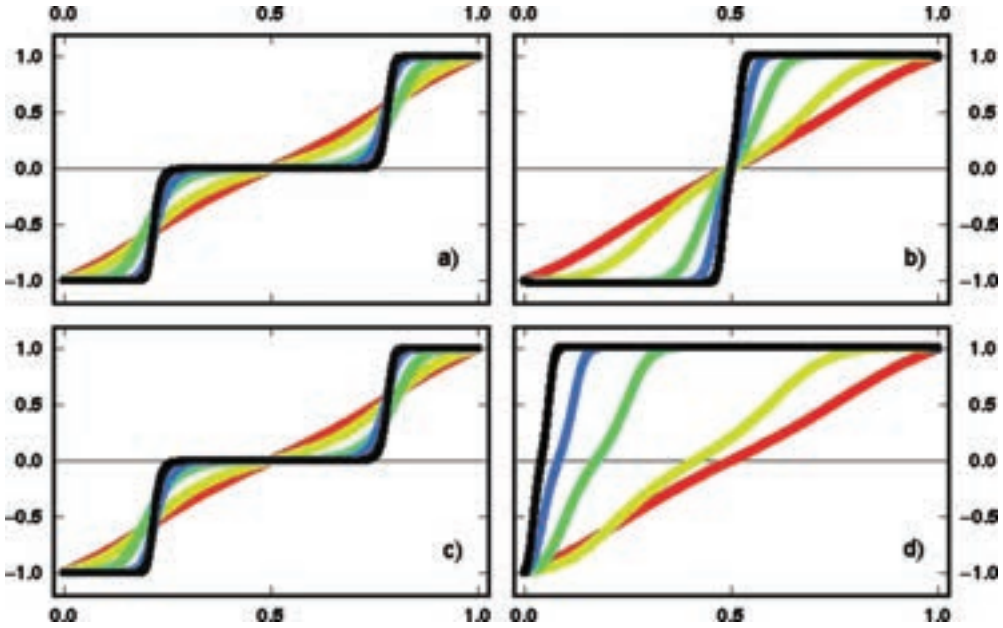

FIG. 1. MPPs for the 1D double-well potential for various path lengths U. The curves correspond to $U=20,10,5,2$, and 1 (black, blue, green, yellow, and red). In panels (a) and (b), the double-well potential was symmetric; in panels (c) and (d), the well depths were slightly different. The temperature for panels (a) and (c) correspond to $\beta=\infty$, and for panels (b) and (d) to $\beta=10$.

with Fig. 1(a); the segmenting remains intact. However for nonzero temperatures, the effects are dramatic. The small asymmetry produces a major asymmetry in the path: Compare Fig. 1(b) with Fig. 1(d). We have taken $\beta=10$ so that the temperature is small compared to the mean energy barrier of size 1 but large compared to the change in $\delta V=0.02$ between end points. At large path lengths the MPP for the asymmetric double well spends almost all of its time at the lower of the two minima. However, when the temperature is much greater than the well-depth difference, according to equilibrium statistical mechanics, the time spent in each well should be about the same; for the parameters chosen, the equilibrium times are approximately 2% different. One way of interpreting the origin of the unphysical nature of the MPPs in the asymmetric case lies in the over reliance of the minimization procedure for I on the minima of G. While equilibrium expectation values satisfy Eq. (5), minimizers of I that concentrate on the minimizers of G may destroy this balance. The tendency of MPPs to minimize G is somewhat pronounced in the asymmetric calculations here and, as we demonstrate below, can be even more problematic in problems of dimension $nd \geq 2$ or more.

B. Example 3.2: Two-dimensional (2D) potential

We consider a 2D problem for a single particle with $2n=d=2$ and

$$V(x_1,x_2) = 4(x_1^2+x_2^2-1)^2x_2^2 - \exp(-4((x_1-1)^2+x_2^2)) - \exp(-4((x_1+1)^2+x_2^2)) + \exp(8(x_1-1.5)) + \exp(-8(x_1+1.5)) + \exp(\alpha(x_2+0.25)) + 0.2\exp(-8x_1^2). \quad (8)$$

This potential has two minima, one maximum, and two saddle points. The choice of $\alpha=-12.163\,839\,304\,988\,416$ ensures that the values of the potential at the two saddle points are identical. For this choice of α, the contours of V are shown in Fig. 2. Note that there are two possible choices for x^0, the saddle point, for which there are pairs of heteroclinic connecting orbits linking x^- to x^+ via x^0. At both minima the potential V takes the value $V_{\min}=-0.9470$. At both saddle points the potential has the value $V_{sp}=-0.1993$.

We use this example to explore the minimization when two routes exist that connect the minima of V. At zero temperature there are two MPPs marked on Fig. 2. We refer to the yellow path as "direct" and the green path as "circular." At zero temperature, both are equally probable because the value of Eq. (6) is the same along either path. Along each route, the path is segmented, spending significant times at the end point minima and at the intervening saddle; refer to the black curves in Fig. 3.

In addition to the zero temperature result, we display both the direct and circular routes at inverse temperatures 100 and 10 in Fig. 3. In all cases the length of the path is such that the segmenting effect is illustrated. However, as the

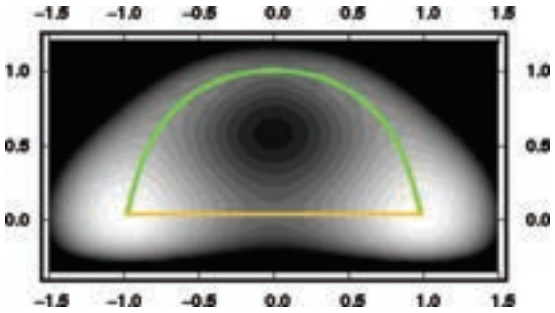

FIG. 2. A contour plot of the 2D potential; see Eq. (8). The two possible transition paths from one minimum to the other are indicated in the figure. The straight yellow line corresponds to the direct route; the green arc denotes the circular route. Along either path the barrier energies are the same.

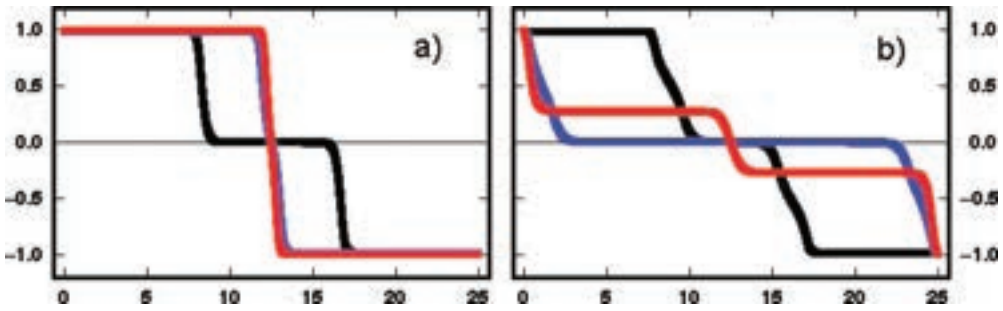

FIG. 3. The x component of the path is plotted as a function of the time u for the direct path (on the left) and the circular path (on the right). The black curve corresponds to the zero temperature path, the blue to $\beta=100$, and the red to $\beta=10$.

temperature is increased from zero, the two routes behave differently. The direct path avoids spending time at the saddle for any positive temperature. This represents the usual instanton picture and occurs because the value of $\Delta V(x^0)$ is negative for the saddle along this route; spending time at the saddle is counter to the minimization of I. The circular route, however, spends significant time at its saddle point; indeed for $\beta=100$ it spends most of its time there. Again this occurs because of the value of $\Delta V(x^0)$ at the saddle, which is positive for this route, and is indeed larger than the value at either minimum. For smaller temperatures, $\beta\approx 10$, the absolute minimum of the path potential G is no longer attained near one of the extrema of the original potential V. This then is reflected in the MPP for the circular route; see Fig. 3. For such temperatures, maximizing the probability is achieved by spending the vast majority of the time at this unphysical point, the absolute minimum of G.

Furthermore, at nonzero temperature, the value of I is consistently lower for the circular route; the MPP analysis assigns a greater probability to this route over the direct route. This, combined with the fact that the circular route spends a long time away from the minima of V, is counterintuitive: It is natural to expect that the circular route, with steeper confining walls, would not be favored over the direct path for entropic reasons. Indeed it is the steep confining walls, which would restrain entropic effects, which lead to the large positive value of ΔV at the saddle on the circular root and lead to smaller values of I than for the direct route. To investigate this point, we looked at the original unconditioned SDE (1), and integrated it forward in time. We looked at the first-passage time: The simulation started with particle in the left well; it finished when the particle crossed the y axis. Over a fairly large range of β, $3<\beta<10$, we found the following. For any particular value of β, both routes had average first-passage times that were almost the same (different by a fraction of a percent). However, the direct route was found to occur more than twice as often; a factor of between 2.0 and 2.2 that was almost constant over this temperature range. This is consistent with physical intuition. The barrier determines the transition time; equal barriers for both routes result in equal transition times. The circular route has the steeper confining "walls" as compared to the direct route; thus the former has a smaller density in pathspace and occurs less often. Thus we infer that the MPP analysis must be treated with caution as it does not encode the entropic effects required to quantify probabilities associated with tubes of likely trajectories in the neighborhood of the MPP. Again the over reliance on the minima of G leads to an unphysical result.

C. Example 3.3: Unbounded path potential *G*

We consider a 2D problem for a single particle with $2n=d=2$ and

$$V(x_1,x_2)=\frac{1}{4}(1-x_1^2)^2+\frac{x_2^2}{2}(1+x_1^2).$$

Straightforward calculation shows that

$$\nabla V=\begin{pmatrix}-(x_1-x_1^3)+x_1x_2^2\\ x_2(1+x_1^2)\end{pmatrix}$$

and

$$\Delta V=4x_1^2+x_2^2.$$

Thus the potential has two minima: at $(x_1,x_2)=(\pm 1,0)$ and a saddle point at $(x_1,x_2)=(0,0)$. The contours are shown in Fig. 4. From this it follows that the path potential satisfies

$$G(0,x_2;\beta)=\left(\frac{1}{2}-\frac{1}{\beta}\right)x_2^2$$

and hence that $G(x;\beta)$ is unbounded from below on $x_1=0$ if $\beta<2$.

The contours of the potential are shown in Fig. 4. A local maximum of the probability that runs along the x_1-axis is

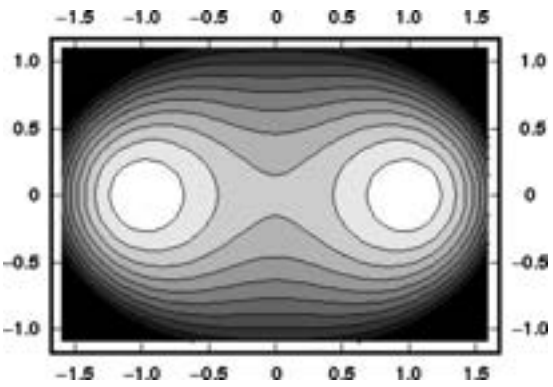

FIG. 4. Contour plot of a simple 2D potential that has an unbounded path potential at high temperature.

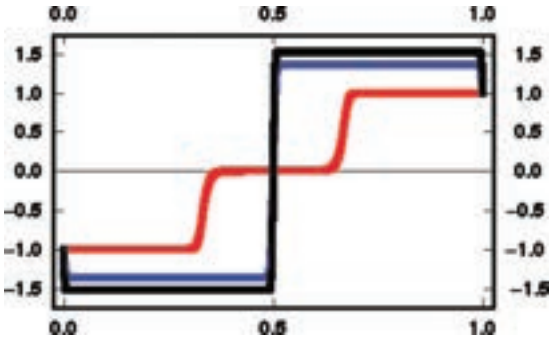

FIG. 5. For Example 3.3, we plot the x_1 component of the path as a function of the time u/U for local minimizers of the path potential. The red curve corresponds to the zero temperature path, the black to $\beta=100$, and the blue to $\beta=10$.

shown in Fig. 5 for inverse temperatures ∞, 100, and 10. In all cases the length of the path is such that the segmenting is illustrated.

However the minimum of I is not finite for this problem. It is possible to choose paths that make large excursions in the x_2 direction, visiting regions where $|G|$ is large and G is negative, that, in turn, makes I negative and large in absolute value. Figure 6 shows three paths found by the minimization routine and corresponding to successively lower values of I given by Eq. (4) as we pass from the white to the blue to the red curves. Further iteration of the minimization algorithm leads to paths that make still larger excursions in x_2 and consequently lead to continued decrease in I. Numerically this appears to continue indefinitely, and thus we encounter yet another unphysical result, which results from the minimization's over-reliance on the minima of G. Note however that we expect entropic effects to eliminate this behavior when the effect of noise is included. In particular, if one looks at a ball of probability centered on a path[11] instead of a path itself (which is a line and hence has zero probability), these long excursions would be seen as extremely unlikely despite the fact that they are minimizers of the Onsager–Machlup potential.

D. Example 3.4: Vacancy diffusion

We consider the case $n=N$ and $d=2$. The force field is similar to that arising in the Lennard-Jones potential (see

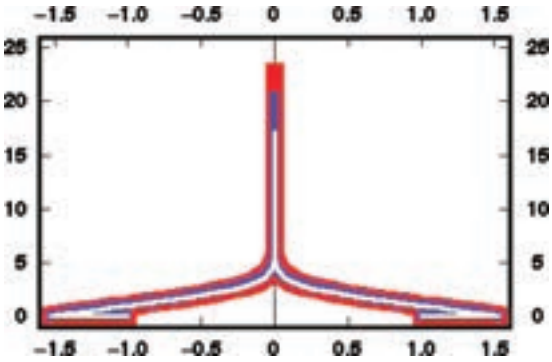

FIG. 6. Again, for Example 3.3, we plot the x_2 component of the path as a function of the x_1 component of the path for a sequence of paths (white, blue, and red), which decrease the path potential. As the iteration scheme continues, the path strays further and further away from the x_1 axis.

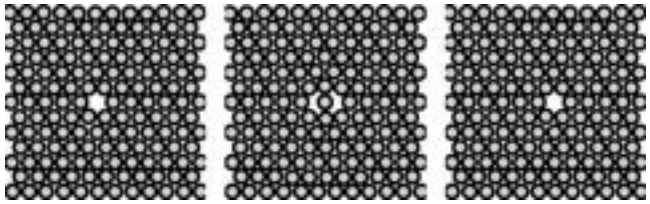

FIG. 7. End point and saddle configurations of the 2D vacancy transition path at zero temperature.

below), but we include only the repulsive component of the potential. Furthermore the N particles are viewed as being arranged periodically and a given particle experiences forces not only from each of the other $N-1$ atoms but also from its periodic images. We have

$$V(x)=\frac{\epsilon}{2}\sum_{k\in\mathbb{Z}^2}\sum_{i\neq j,i,j=1}^{N}\left(\frac{l}{r_{ij}^k}\right)^{12}, \tag{9}$$

where

$$r_{ij}^k=|x_i-x_j-k\xi|$$

and, for fixed $k\in\mathbb{Z}^2$, $k\xi$ denotes the vector displacement of a given periodic image, with ξ the appropriate scale factor. Here $|\cdot|$ denotes Euclidean distance.

At a temperature of one ($\beta=1$), such a system melts at density of $\rho^*=1.006$; see Ref. 18. We take the lattice spacing corresponding to this density and create boxes that contain 1560 lattice sites (39×40), and we use periodic boundary conditions to simulate an infinite system. We have removed one atom and created a vacancy. Under unconditioned Brownian dynamics, the atoms surrounding the vacancy moved slightly toward the open region created by the vacancy, but vacancy diffusion does not occur on reasonable time-scales at low temperature.

We condition on the event that the vacancy moves to the left by one atomic spacing; this corresponds to specifying x^+ in Eq. (2). As shown in the Fig. 7, the beginning and ending states, x^- and x^+, respectively, are different only in that the vacancy is displaced by one lattice site. (The atoms are free to move anywhere in space, and we use the word lattice only because of the structure of the ground state.) At zero temperature $\beta=\infty$ and with $\rho^*=1.006$, we minimize $I_0(x)$. The path so determined contains no surprises. An atom neighboring the vacancy moves in a straight line into the empty space, leaving behind a displaced vacancy. The atom is allowed to move, i.e., minimizing the energy barrier, only because a channel is created by a collective motion of the other nearby atoms, as shown in the middle panel of Fig. 7. The resulting energy barrier is shown in Fig. 8, the height $E_b=1.13$. Since the starting and ending states have the same energy, the resulting (effective) one-body confinement potential experienced by the particle, which diffuses into the vacancy, is a simple symmetric double well. The disturbance is quite localized; we found very small displacements for atoms four or five lattice spacings away from the vacancy. The path shows the segmenting behavior for $U=9$.

At nonzero temperature ($\beta<\infty$), the results of minimizing I given by Eq. (4) to generate the MPP are interesting. As

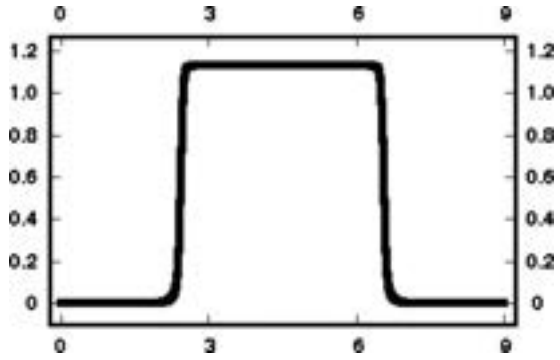

FIG. 8. Energy along the path for the 2D vacancy problem at zero temperature.

with the circular route in Example 3.2, the value of the trace of the Hessian of V plays a major role in determining minimizers of I. This is illustrated in Fig. 9 with $\beta=10$ and $\rho=\rho^*$. Note that the energy scale is a factor of 20 larger than that used in the previous plot, Fig. 8. The saddle state is best characterized by recognizing that two disclinations are present, shown in Fig. 10. For the vast majority of the time along the path, the system resides in this barrier (saddle) state, as shown in Fig. 9. Again the over-reliance of the minima of G is responsible for this counterintuitive behavior in the MPP, which spends a large amount of time along the path at the larger energy state (the saddle), compared to the time spent at the energy minima.

E. Example 3.5: Lennard-Jones molecules

We consider the case $n=N$ and $d=2$ ($d=3$) for which the jth particle $x^{(j)} \in \mathbb{R}^2$ ($\mathbb{R}^3$). We use the notation $r_{ij}=|x^{(i)}-x^{(j)}|$ to denote the Euclidean distance between the ith and jth particles. Then the Lennard-Jones potential is made from a sum of pairwise interactions between the particles,

$$V(x) = 2\epsilon \sum_{i\neq j,i,j=1}^{N} \left[\left(\frac{l}{r_{ij}}\right)^{12} - \left(\frac{l}{r_{ij}}\right)^{6} \right]. \tag{10}$$

We look at two types of Lennard-Jones clusters, studying seven atoms in a plane, and 38 atoms in three-dimensional physical space. In so doing we again show that many of the ideas illustrated on the simple 1D and 2D test problems can be carried over to these more complex models in 2×7 and

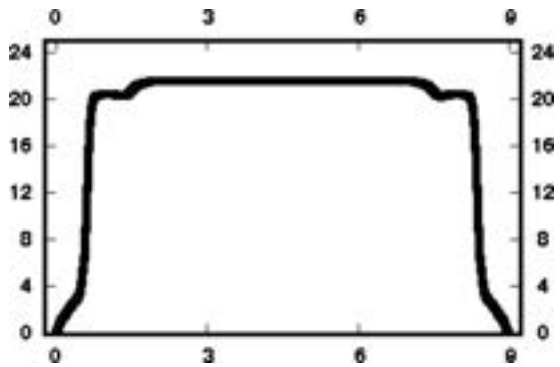

FIG. 9. At $\beta=10$, energy along the path (as a function of u) for the 2D vacancy problem.

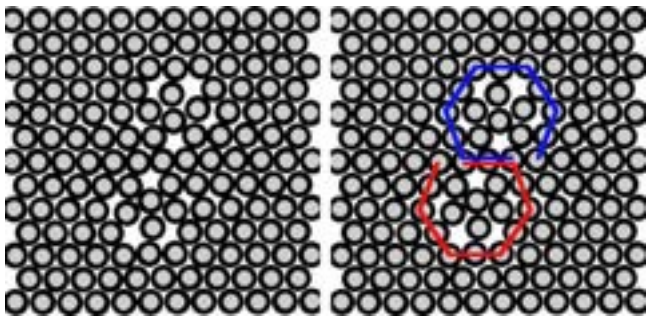

FIG. 10. At $\beta=10$, the barrier saddle configuration, with (right) and without (left) disclinations highlighted. This state persists for the majority of the time (along the path). In particular, in the minimization procedure for $U=9$, this is the state visited in the middle five time units (see previous figure).

3×38 dimensions, respectively, as they can be for the vacancy diffusion problem. The 2D seven-atom Lennard-Jones cluster is studied in Ref. 19. The Lennard-Jones 38 problem is studied in Refs. 20–25.

F. Seven atoms

In two dimensions, the ground state of the seven-atom Lennard-Jones cluster consists of a central atom surrounded by six others. One of the questions we ask is: What is the pathway for the central atom to migrate to the surface as in Ref. 19? Here we investigate one such path for several temperatures; see Fig. 11 for the transition states. We plot the energy of the configurations along the path in Fig. 12. All of the curves are segmented, spending significant time in which the configuration is changing very little, namely, the transitions states shown in Fig. 11. At zero temperature (the black curve in Fig. 11), we obtain results that are similar to those found in Ref. 19. At nonzero temperatures the curve shows significant differences from that found at zero temperature. At $\beta=20$ and $\beta=5$ the path spends the vast majority of the time in the close-packed state: A central atom surrounded by six atoms. Indeed the dominant states here are simply configurations obtained by expanding the boundary configurations of the zero temperature path. At $\beta=2.5$ a different state dominates. This state is one of the transition states seen at zero temperature and is shown in configuration number 3 in

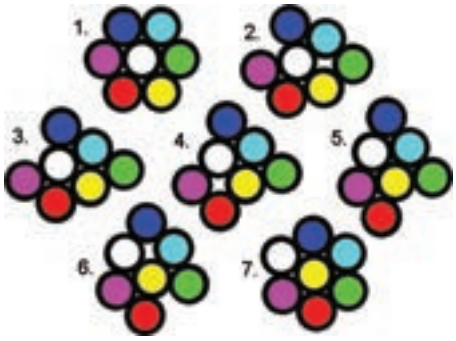

FIG. 11. The various configurations corresponding to the states seen in the zero temperature MPP for the seven-atom Lennard-Jones cluster. States 1 and 7 are the imposed boundary conditions, again related to each other by symmetry. States 3 and 5 are local energy minima, again symmetry related to each other. States 2 and 6 are symmetry related saddles. State 4 is the barrier saddle.

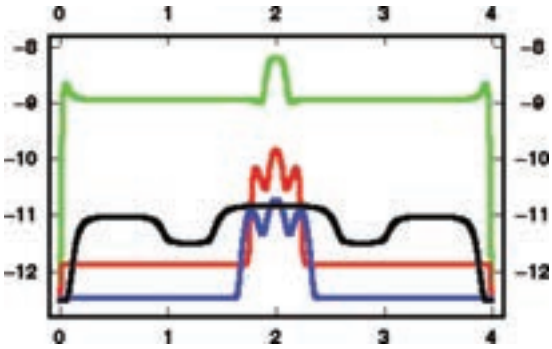

FIG. 12. Energy along the MPP (as a function of u) for the seven-atom Lennard-Jones cluster. The black corresponds to $\beta=\infty$, blue to $\beta=20$, red to $\beta=5.0$, and green to $\beta=2.5$.

Fig. 11. This new predominant state can be described in terms of three rows: two rows of three atoms capped by a single atom, asymmetrically placed, i.e., one of the metastable states found in Ref. 19. We interpret this as a mean-field approximation to a conformation change induced by the increased temperature. The path potential G has more than one minimum; as a function of temperature, the global minimum jumps from one minimum to another. Minimizing I then produces a path that spends as much time as possible at the global minimum. The physical information contained in such a transition temperature calculation is unclear precisely for the reasons elucidated on the simpler model problems discussed earlier.

G. 38 atoms

We now consider a cluster of 38 Lennard-Jones atoms. The ground state and the first excited state for packing 38 such atoms are found to have very different symmetries: O_h and C_{5v}, respectively. We consider paths whose starting configuration is the ground state and ending configuration is the first excited state. Figure 13 illustrates segmenting, showing that at zero temperature and for sufficiently long paths, MPPs are essentially piecewise constant and concentrated at critical points of the potential. Indeed the path for $U=25$ gives a value of I close to that predicted by the sum rule, Eq.

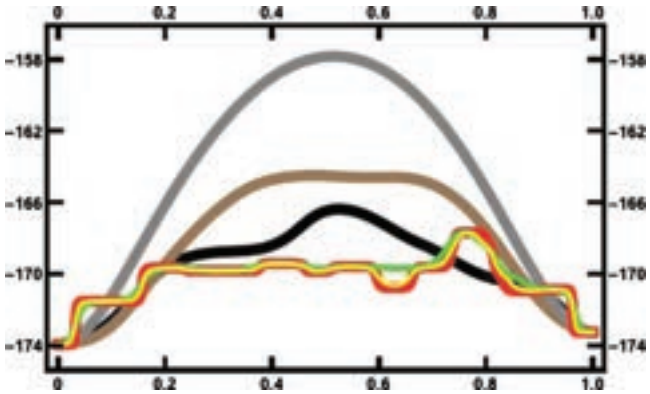

FIG. 13. The energy along the path (as a function of u/U) for the 38-atom Lennard-Jones cluster at zero temperature. The different curves correspond to differing values of the path length U. Gray is used for the shortest value of $U=0.1$, red for the longest, $U=25$; the brown, black, green, and yellow curves correspond to intermediate values of U.

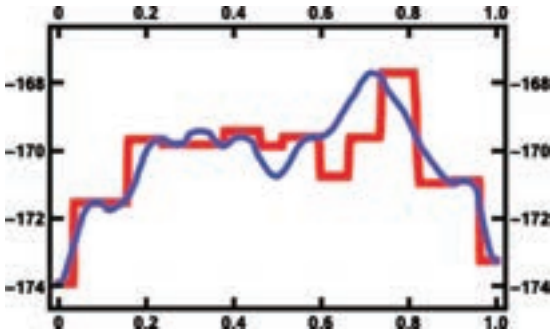

FIG. 14. The energy along the path (as a function of u/U for the 38- atom Lennard-Jones cluster. The smoother blue curve corresponds to the path that was used as the starting point of the minimization procedure (Ref. 25). The red curve corresponds to the final result of the minimization procedure for $U=25$, the same as the red curve in the previous figure. Note that the minimization procedure started with a smooth curve and produced one with sharp transitions between states.

(6). However short paths lose the interesting structure and approach a parabolic limit as the path length shrinks. Figure 14 shows how the zero temperature path with $U=25$ compares with the transition path obtained by other techniques.[26] Indeed our algorithm takes this previously published path[25] as a starting point in our descent algorithm to maximize probability. Notice that the segmenting is absent in the starting path; the segmenting is a consequence of the minimizing I_0.

Figure 15 shows the energy along the path at two finite temperatures of $\beta=50$ and $\beta=20$. The complex transition structure, which is present at zero temperature (see Fig. 14), is greatly modified, and in each case, a single state dominates. In both cases the dominant state is an expanded state of one of the end point zero temperature configurations; however the preferred end state differs between the two temperatures. All the transitions occur in a small fraction of the path, with a single state dominating most of the path. Increasing the path length U does little to change the overall picture; simply more time will be spent in the dominant state. The over-reliance of the minimization on the minima of G again manifests itself here: The MPPs are extremely sensitive to the difference in such minima. The length of time spent in a state has only a tenuous connection to reality since

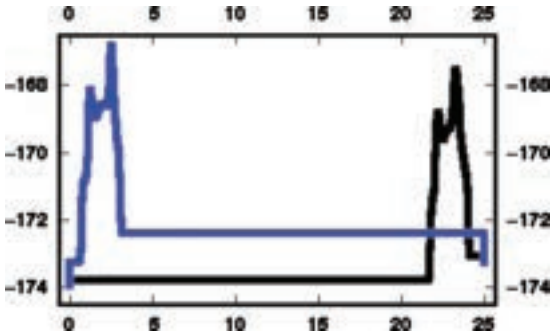

FIG. 15. The energy along the path (as a function of u) for the 38-atom Lennard-Jones cluster at nonzero temperature. The black curve for $\beta=50$ is dominated by a state similar to the ground state the long flat portion on the left. The blue curve, $\beta=20$, is dominated by a state similar to the first excited state: The long flat portion on the right.

the minima of the path potential G constitute a small set of configurations that do not reflect the equilibrium thermodynamic properties of the system.

IV. SUMMARY AND DISCUSSION

In this paper, we have explored the dominant transition paths generated by Brownian dynamics for a range of model problems, studying the role of finite large temperature in transitions constrained to occur on a finite but large time interval. Some of the effects uncovered here are indeed artifacts of the particular 1D and 2D models we have constructed. Yet, these 1D and 2D models are also robust enough to explain much of the behavior of the MPPs we have demonstrated in the more complicated and physically motivated models such as vacancy diffusion and Lennard-Jones clusters. For such paths we have found a number of interesting phenomena.

(1) *Segmenting*: The fact that on long enough domains, the MPPs segment into paths, which are approximately constant, together with rapid transitions between them. However, on paths that are short, different effects are observed, and the paths do not segment into piecewise constant transitions.
(2) *Asymmetry*: The fact that even a tiny asymmetry can, at finite temperature, drive MPPs to spend most time at one well over another.
(3) *Multiple routes*: The fact that in complex energy landscapes, there may be multiple routes through phase space based on the idea of connecting critical points through sharp transitions. This is related to the choice of critical point (usually a saddle) x^0 through which the transition path passes.
(4) *Saddle effect*: The fact that the contribution ΔV to the path potential G can, at finite temperature, drive the MPP to spend most time at one critical point of V over another. Furthermore it is possible for the MPP to spend most of its time at a saddle point and not at minima, a physically counterintuitive behavior. In particular the preference for trajectories that reside at saddle points for long times is most pronounced on trajectories where entropic effects would be expected to be small rather than large.
(5) *Boundary values*: The fact that at finite temperature boundary conditions at minima of V seem unnatural; minima of the path potential G are more natural. However, the minima of $G(\cdot;\beta)$ are not a good representation of the thermally accessible configurations.
(6) *G not bounded from below*: The fact that for some problems, G is not bounded from below and the effect that this has on MPPs. This is a situation where the transition paths may make large excursions from the neighborhood of critical points of V in order to minimize $G(\cdot;\beta)$. We emphasize, again, that the minima of $G(\cdot;\beta)$ are not a good representation of the thermally accessible configurations.

In particular, we would like to point out that as with all mean-field approaches, the approximation made by neglecting the effect of noise on the paths produces features that may or may not be useful in describing the actual Brownian dynamics. Understanding these possible pitfalls that underlie the use of MPPs will provide the tools to better evaluate the usefulness of such methods. As discussed here and by Sega *et al.*,[12] the (trace of the) Hessian of the particle potential V plays an important role in determining which states dominate the minimization procedure. However, the minimization emphasizes configurations where the value of the path potential G is a minimum. This is in direct contrast to what is expected when noise is included since, in thermal equilibrium, Eq. (5) must hold. As indicated by Durr and Bach,[11] one must look for the maximum probabilities of a ball in pathspace. However taking the limit and looking at the line of maximal probability are fraught with pitfalls. Here we have shown examples where the MPPs, lines that come from minimizing the relevant Onsager–Machlup action, do not correspond to the maximum flux. Thus one must be wary of the MPPs generated from such a minimization procedure. The MPPs *may* contain useful physical information but must be treated cautiously to avoid making erroneous deductions. Our work clearly demonstrates a number of unphysical effects that can be present in MPPs and explains their origin. We now consider the implications of our results for the interpretation of other recent work.

First consider the article by Minh and Adib[27] in which a path integral analysis of Jarzynski's equality is undertaken. This analysis explored minimizing functions that are similar to the integral I_0 in Eq. (4) above and hence may suffer from the same problems as we demonstrate in this paper. In the 2D model's case, where the path potential, G, was unbounded, minimizing either of the functions considered in Ref. 27 would lead to results that would be difficult to interpret physically: such minimization procedures would lead to paths dominated by the regions far away from any particle potential minima, where the path potential is large (in absolute value). In addition, our other 2D model (Example 3.3), where two paths are present, using the analysis in Ref. 27 would also produce an unphysical result unless the pulling potential (time dependent) were to be unusually large.

In a recent article, Autieri *et al.*[14] investigated pathways in high-dimensional systems. There the suggestion is made that the boundary conditions can be set at positions that correspond to minima of the path potential, G. The lessons from our work show that this may lead to unphysical effects. In the 2D model with two paths, many minima of G exist, and the absolute minimum does not usually correspond to a minima of the original particle potential. Now consider the case, studied above, of vacancy diffusion (Example 3.4) in 2D. It is only at very low temperatures ($<0.1T_m$, where T_m is the melting temperature) that the configuration that minimizes G looks like the ground state, namely, a "perfect" lattice with a single vacancy. As described above, the absolute minimum of G appears at a saddle point of the particle potential.

In the same paper[14] the authors discussed the time evolution of the MPPs. There the authors attributed physical meaning to the length of time that the path spends at each minimum. Our analysis above shows that these cannot be

taken, in general, to be physical times. In particular, consider the 1D Example 3.1, with a small asymmetry, δE. When the temperature is large compared to the asymmetry but small compared to ΔE the barrier energy, $\delta E \ll k_B T \ll \Delta E$, our analysis shows that the path spends an exponentially long time in the deeper well. Paths that are sufficiently long should capture the essence of equilibrium thermodynamics for which the times spent in each well are almost identical.

Finally, we turn to the work of Malinin and Chernyak[28] who investigated the transition times in the low-noise limit of Brownian dynamics. We would like to address two points in relation to our work. First we note that the work[28] describes a perturbative method that uses MPPs as the starting points. Thus it is desirable to ensure that the properties of the MPPs are physical. This, as seen above, may not be the case. Next consider the path potential; it breaks up naturally into two parts, one independent of the temperature and the other dependent. However, as discussed above, in equilibrium, the thermodynamic average of both parts are comparable to one another in magnitude, which leads to the thermodynamic average of G itself being $\langle G \rangle = -k_B T \langle \Delta V \rangle / 2$, proportional to the product of both the temperature and to the Laplacian of the particle potential. For the 38-atom Lennard-Jones cluster, the Laplacian at the ground state is on the order of 2×10^4 and remains at similar levels over the MPP. Thus only at temperatures much smaller than 10^{-4} is it an accurate approximation to eliminate the Laplacian in the path potential. Malinin and Chernyak omitted the Laplacian contribution in their analysis at the saddle, and thus they considered a zero temperature limit rather than simply a small noise limit. See the paper by Adib[29] for further discussion of the importance of the Laplacian contribution to the path potential. For the 38-atom cluster studied here, Malinin and Chernyak's analysis is only valid at very low temperatures, $<10^{-4}$, whereas the temperature of interest is of the order of 0.1 for transitions between the lowest states of cluster.

[1] P. Bolhuis, C. Dellago, P. L. Geissler, and D. Chandler, Annu. Rev. Phys. Chem. **53**, 291 (2002).
[2] H. Waalkens, R. Schubert, and S. Wiggins, Nonlinearity **21**, R1 (2008).
[3] H. Schwetlick and J. Zimmer, J. Chem. Phys. **130**, 124106 (2009).
[4] A. Ghosh, R. Elber, and H. A. Sheraga, Proc. Natl. Acad. Sci. U.S.A. **99**, 394 (2002).
[5] W. E, W. Ren, and E. Vanden-Eijnden, Phys. Rev. B **66**, 052301 (2002).
[6] W. E, W. Ren, and E. Vanden-Eijnden, J. Phys. Chem. B **109**, 6688 (2005).
[7] W. E, W. Ren, and E. Vanden-Eijnden, Chem. Phys. Lett. **413**, 242 (2005).
[8] R. Olender and R. Elber, J. Mol. Struct.: THEOCHEM **63**, 398 (1997).
[9] P. Faccioli, M. Sega, F. Pederiva, and H. Orland, Phys. Rev. Lett. **97**, 108101 (2006).
[10] M. I. Freidlin and A. D. Wentzell, *Random Perturbations of Dynamical Systems* (Springer-Verlag, New York, 1984).
[11] D. Dürr and A. Bach, Commun. Math. Phys. **60**, 153 (1978).
[12] M. Sega, P. Faccioli, F. Pederiva, G. Garberoglio, and H. Orland, Phys. Rev. Lett. **99**, 118102 (2007).
[13] P. Faccioli, J. Phys. Chem. B **112**, 13756 (2008).
[14] E. Autieri, P. Faccioli, M. Sega, F. Pederiva, and H. Orland, J. Chem. Phys. **130**, 064106 (2009).
[15] F. J. Pinski, A. M. Stuart, and F. Thiel (in preparation).
[16] P. Pulay, Chem. Phys. Lett. **73**, 393 (1980).
[17] A. J. Bray and A. J. McKane, Phys. Rev. Lett. **62**, 493 (1989).
[18] J. Q. Broughton, G. H. Gilmer, and J. D. Weeks, Phys. Rev. B **25**, 4651 (1982).
[19] C. Dellago, P. Bolhuis, and D. Chandler, J. Chem. Phys. **108**, 9236 (1998).
[20] M. R. Hoare and P. Pal, Adv. Phys. **20**, 161 (1971).
[21] M. R. Hoare and P. Pal, Nature (London), Phys. Sci. **230**, 5 (1971).
[22] M. R. Hoare and P. Pal, Nature (London), Phys. Sci. **236**, 35 (1972).
[23] F. M. Torres, E. Agichtein, L. Grinberg, G. Yu, and R. Q. Topper, J. Mol. Struct.: THEOCHEM **419**, 85 (1997).
[24] J. P. Doye, M. A. Miller, and D. J. Wales, J. Chem. Phys. **110**, 6896 (1999).
[25] S. A. Trygubenko, http://pdb.trygub.com/pathways/lennard-jones/38/global-second-lowest/3-274sigma/largest-rate-contribution/path-xyz.bz2, 2006.
[26] J. P. Doye, "The structure, thermodynamics and dynamics of atomic clusters," Ph.D. thesis, University of Cambridge, United Kingdom, 1996; see http://physchem.ox.ac.uk/doye/jon/PhD2/PhD.html.
[27] D. D. L. Minh and A. B. Adib, Phys. Rev. E **79**, 021122 (2009).
[28] S. V. Malinin and V. Y. Chernyak, J. Chem. Phys. **132**, 014504 (2010).
[29] A. B. Adib, J. Phys. Chem. B **112**, 5910 (2008).